



# An experimental investigation of flow fields near a liquid–liquid moving contact line

Charul Gupta<sup>1,a</sup>, Lakshmana D. Chandrala<sup>1,b</sup>, and Harish N. Dixit<sup>1,2,c</sup> 

<sup>1</sup> Department of Mechanical & Aerospace Engineering, Indian Institute of Technology Hyderabad, Kandi, Sangareddy, Telangana 502284, India

<sup>2</sup> Centre for Interdisciplinary Programs, Indian Institute of Technology Hyderabad, Kandi, Sangareddy, Telangana 502284, India

Received 16 January 2024 / Accepted 12 April 2024 / Published online 26 April 2024

© The Author(s), under exclusive licence to EDP Sciences, Springer-Verlag GmbH Germany, part of Springer Nature 2024

**Abstract** A moving contact line occurs at the intersection of an interface formed between two immiscible liquids and a solid. According to viscous theory, the flow is entirely governed by just two parameters, the viscosity ratio,  $\lambda$ , and the dynamic contact angle,  $\theta_d$ . While a majority of experimental studies on moving contact lines involve determining the relationship between the dynamic contact angle and capillary number, a few studies have focused on measuring the flow field in the vicinity of the contact line involving liquid–gas interfaces. However, none of the studies have considered liquid–liquid moving contact lines and the present study fills this vital gap. Using particle image velocimetry, we simultaneously measure the velocity field in both the liquid phases using refractive index-matching techniques. The flow field obtained from experiments in both phases is directly compared against theoretical models. Measurement of interface speed reveals that material points rapidly slow down as the contact line is approached. Further, the experiments also reveal the presence of slip along the moving wall in the vicinity of the contact line suggesting a clear mechanism for how the singularity is arrested at the contact line.

## 1 Introduction

The dynamics of liquid–gas moving contact line is a classical problem in fluid mechanics and has been discussed extensively in several reviews [1–5]. The problem attracted a lot of attention owing to the singularity at the moving contact line when the standard boundary condition of ‘no-slip’ is applied on the moving wall. The presence of the singularity was first recognized by Huh and Scriven [6] (HS71 hereafter), wherein the authors obtained a ‘local’ solution in the vicinity of the contact line by assuming the interface to be flat. In the viscous limit, HS71 theory predicts three different flow regimes based on the value of the viscosity ratio,  $\lambda = \mu_1/\mu_2$ , and the dynamic contact angle,  $\theta_d$ . In a recent study [7], we showed that the HS71 theory quantitatively predicts the flow field away from the moving contact line, but the experiments were restricted to liquid–gas systems only. There are very few experimental studies involving a moving contact line formed in a liquid–liquid system [8, 9], but these too are restricted to measuring the dynamic contact angle without any information about the flow field in the two liquids. There are two challenges involved in determining the flow field in liquid–liquid moving contact lines. The first is the high-resolution needed to test viscous theories which are essentially local in nature, and the second is the ability to measure flows in both fluids simultaneously.

In the present study, we conduct particle image velocimetry (PIV) experiments in a liquid–liquid moving contact line for viscosity ratio,  $\lambda \geq 1$ . The primary objective of the study is to measure the flow field in both liquids simultaneously using a refractive index (RI)-matched PIV technique and compare the results against theoretical predictions. The secondary objective is to measure flow along the interface as well as the moving plate to determine how the singularity at the moving contact line, present in HS71 theory, is resolved.

The experimental parameters in the present study could also be of interest to the modelling community. Numerical simulations involving moving contact lines are particularly challenging when there is a large contrast between

<sup>a</sup> e-mail: [me18resch11001@iith.ac.in](mailto:me18resch11001@iith.ac.in)

<sup>b</sup> e-mail: [lchandrala@mae.iith.ac.in](mailto:lchandrala@mae.iith.ac.in)

<sup>c</sup> e-mail: [hdixit@mae.iith.ac.in](mailto:hdixit@mae.iith.ac.in) (corresponding author)

the density and viscosity ratio. As a result, several studies, especially those relying on phase-field models, have focused on systems where the viscosity ratio is close to unity [3, 10]. The parameters used in the present study make it now possible to validate the numerical results against the experiments quantitatively.

The paper is organized as follows: in Sect. 2, we discuss the experimental setup and the investigated parameter regimes. After a brief review of relevant theoretical models in Sect. 3, the results are presented in Sect. 4. We summarize key observations and the outcomes of the study in Sect. 5.

## 2 Experimental setup and parameter regimes

The experimental setup shown in Fig. 1a consists of a transparent rectangular tank of dimensions  $200\text{ mm} \times 100\text{ mm} \times 27\text{ mm}$  filled with two immiscible liquids. Standard PIV optics involving a 2W continuous diode laser and a set of a bi-convex spherical lens and plano-convex cylindrical lens generate a thin laser sheet of approximately 0.5 mm thickness. A 1 MP high-speed Photron Nova S9 camera with a macro lens captures images at frame rates of 50–500 fps depending upon the speed of the slide. The field of view is varied between  $5.1\text{ mm} \times 5.1\text{ mm}$  to  $7.9\text{ mm} \times 7.9\text{ mm}$  to obtain the flow fields in both phases with spatial resolution of  $\approx 5\text{ }\mu\text{m}/\text{pixel}$  to  $8\text{ }\mu\text{m}/\text{pixel}$ , respectively. A traverse loaded with a vertical glass slide is immersed in the tank at a controlled speed. To keep the contact line and interface position fixed during imaging, liquid from the bottom of the tank was removed at a prescribed rate using a programmable syringe pump. Two different kinds of seeding particles  $2\text{ }\mu\text{m}$  for sugar–water mixture and  $5\text{ }\mu\text{m}$  for silicone oil are utilized to capture the flow near the contact line.

In order to allow the laser sheet to pass through both liquids without any distortion or reflections from the interface, both fluids must have the same refractive index. First, polydimethylsiloxane (silicone oil) of a known viscosity is chosen and then the sugar–water mixture is prepared such that its refractive index matches that of silicone oil. Since the refractive index of the sugar–water mixture varies as the concentration of sugar changes, an appropriate concentration of sugar is chosen till the refractive index of the sugar–water mixture matches with that of the silicone oil. A separate batch of sugar–water mixture was prepared for every batch of silicone oil. The properties of each liquid are given in Table 1 and the properties of the liquid–liquid combination are given in Table 2. Since the density of the sugar–water mixture was always higher than that of the silicone oil, fluid-1 (upper fluid)

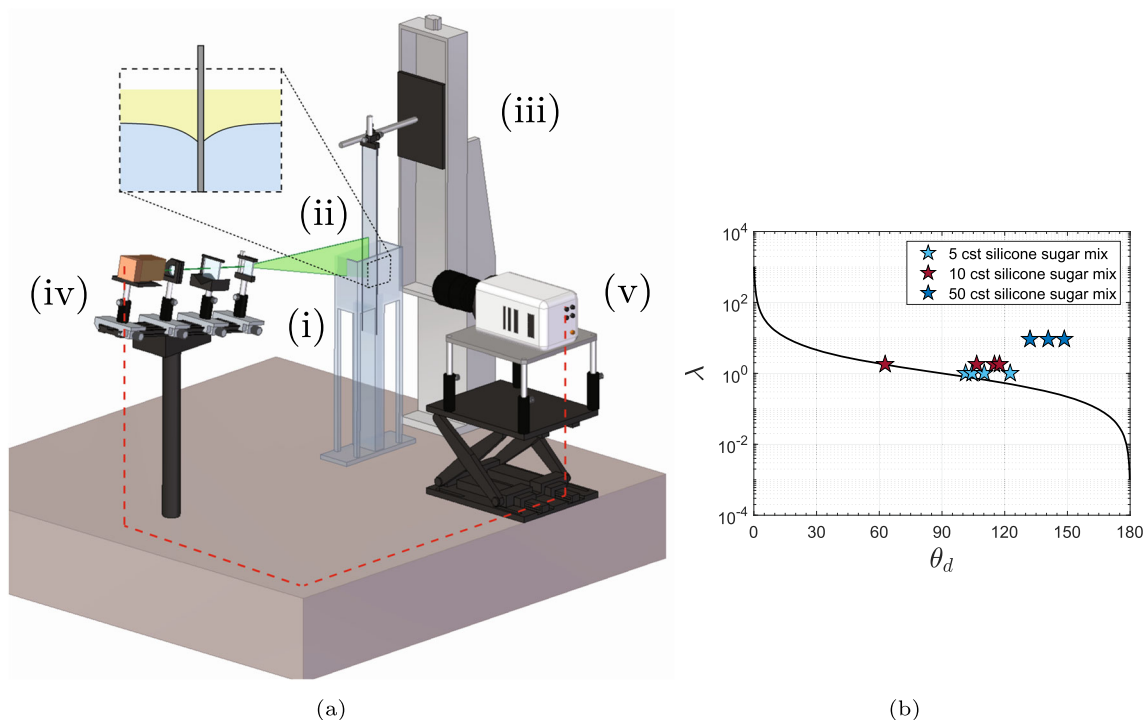


**Fig. 1** **a** A schematic illustration of the experimental setup and 2D PIV measurement system. (i) Rectangular tank containing two immiscible liquid phases (indicated in the inset). (ii) Glass plate. (iii) Linear motorized traverse. (iv) Laser along with sheet optics. (v) High-speed camera with a macro lens. **b** Phase plot of viscosity ratio and dynamic contact angle plane. The black solid curve represents the theoretical critical viscosity ratio curve predicted by Huh and Scriven [6]. The symbols indicate the experimental data points

**Table 1** Properties of fluids used in experiments

	Density, kg/m <sup>3</sup>	Viscosity 10 <sup>-3</sup> , Pa s	Surface tension, mN/m
Air	1.207	0.0189	–
Water	1000	0.89	72
SW-1 <sup>a</sup> : Sugar–water mixture	1176	4.54	75.1
SW-2 <sup>a</sup> : Sugar–water mixture	1180	4.9	75.1
5 cSt Silicone oil	913	4.56	19.5
10 cSt Silicone oil	940	8.8	19.5
50 cSt Silicone oil	970	46.1	19.5

<sup>a</sup>SW represents refractive index (RI)-matched sugar–water mixtures

**Table 2** Properties of liquid–liquid combinations

Fluid-1	Fluid-2	Density difference $\Delta\rho$ , kg/m <sup>3</sup>	Interfacial tension $\gamma$ , mN/m	$\lambda = \mu_1/\mu_2$	$l_c = \sqrt{\frac{\gamma}{\Delta\rho g}}$ (mm)	$n$ (RI)
5cSt Si oil	SW-1	263	35.03	1	3.68	1.3990
10cSt Si oil	SW-2	240	37.04	1.8	3.96	1.4010
50cSt Si oil	SW-2	210	36.50	9.4	4.20	1.4024

was always silicone oil and fluid-2 was the refractive index-matched sugar–water mixture. Since the glass slide was always made to slide downwards, silicone oil becomes the displaced (receding) fluid and the sugar–water mixture becomes the displacing (advancing) fluid. The viscosity ratio, defined as  $\lambda = \mu_1/\mu_2$ , was always found to be higher than one in the present study.

While matching the refractive index is the best way to conduct PIV experiments in both liquids, the interface disappears from direct visual sight. As a result, the interface position is determined by carefully tracing the particle paths as described below. To obtain the vector fields from particle images, preprocessing of the images is performed including average background subtraction and image equalization. Particle images are processed using a multi-grid, window-deforming PIV algorithm. The signal-to-noise ratio was improved using an ensemble PIV correlation in an interrogation window of 8 pixels  $\times$  8 pixels. The interface shapes were extracted by analysing particle paths and the interface position was determined with the help of a streakline image obtained by combining about 500 consecutive images. This technique works only when the flow is strictly two dimensional and steady as is the case in the present study.

A cleaning protocol was strictly followed in all experiments to avoid any contamination. Before starting the experiments, the tank and glass slides were cleaned with isopropyl alcohol, followed by a thorough rinse with distilled water, and dried using a hot air gun to avoid any potential contamination. To control the contact angle, either hydrophilic or hydrophobic coatings were applied on the glass surface. After allowing the coating to dry, the slides were thoroughly rinsed in distilled water to remove any loose particles from the coating and then dried. Experiments were conducted only after the glass slides reached ambient temperatures to prevent any thermal Marangoni effects.

The speed of the glass slide was independently varied to achieve various Reynolds and capillary numbers as given in Table 3. The Reynolds and capillary numbers are defined in terms of the lower fluid, i.e. sugar–water mixture, the interfacial tension, and the capillary length. This is consistent with liquid–gas experiments [7, 11] where Re and Ca are also defined using the properties of the lower fluid. A phase plot showing all the experimental data points is shown in Fig. 1b. Figure 2 shows streakline images with a silicone oil/sugar-water/glass system. The streakline image is obtained by combining the 500 particle images spanned over 2 s of real-time. Only those particle images are considered which are captured after reaching a steady state.

**Table 3** Operating parameters

Fluid combination	$U$ (mm/s)	Re	Ca	Contact angle ( $^{\circ}$ )	Surface property
Combination-1: 5 cSt silicone oil (fluid-1) & SW-1 (fluid-2)	0.5	$4.77 \times 10^{-1}$	$6.48 \times 10^{-5}$	$\approx 101.3$	Uncoated
	1	$9.53 \times 10^{-1}$	$1.30 \times 10^{-4}$	$\approx 122.6$	Coated
	1	$9.53 \times 10^{-1}$	$1.30 \times 10^{-4}$	$\approx 104.4$	Uncoated
	5	4.77	$6.48 \times 10^{-4}$	$\approx 110.2$	Uncoated
Combination-2: 10 cSt silicone oil (fluid-1) & SW-2 (fluid-2)	0.5	$4.77 \times 10^{-1}$	$6.61 \times 10^{-5}$	$\approx 62.8$	Coated
	1	$9.54 \times 10^{-1}$	$1.32 \times 10^{-4}$	$\approx 106.6$	Coated
	5	4.77	$1.19 \times 10^{-3}$	$\approx 115.1$	Coated
	5	4.77	$1.19 \times 10^{-3}$	$\approx 117.5$	Uncoated
Combination-3: 50 cSt silicone oil (fluid-1) & SW-2 (fluid-2)	0.15	$1.52 \times 10^{-1}$	$2.01 \times 10^{-5}$	$\approx 132.1$	Coated
	0.5	$5.07 \times 10^{-1}$	$6.71 \times 10^{-5}$	$\approx 140.8$	Coated
	1	1.01	$1.34 \times 10^{-4}$	$\approx 148.5$	Coated

Uncoated represents a clean glass surface. Coated represents a coated surface with hydrophilic coating

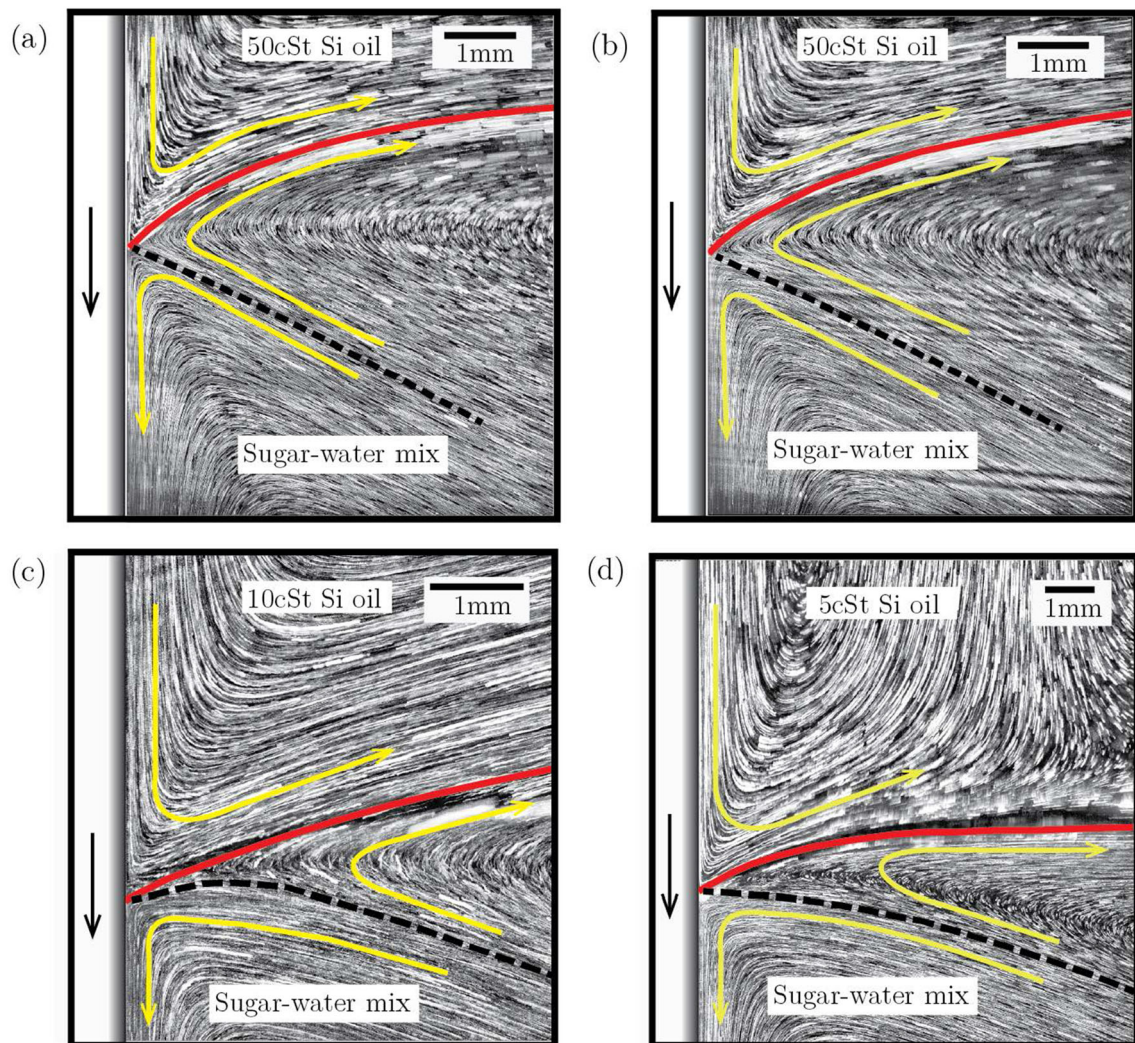


**Fig. 2** Experimental streakline images showing the flow patterns for different liquid–liquid systems ( $\lambda \approx 9.4$  for **a** and **b**;  $\lambda \approx 1.8$  for **c** and  $\lambda \approx 1$  for **d**). The red solid line represents the interface between the silicone oil and sugar–water phases. The yellow arrow represents the direction of the flow in both phases. The black dashed line indicates the split-streamline in the sugar–water phase

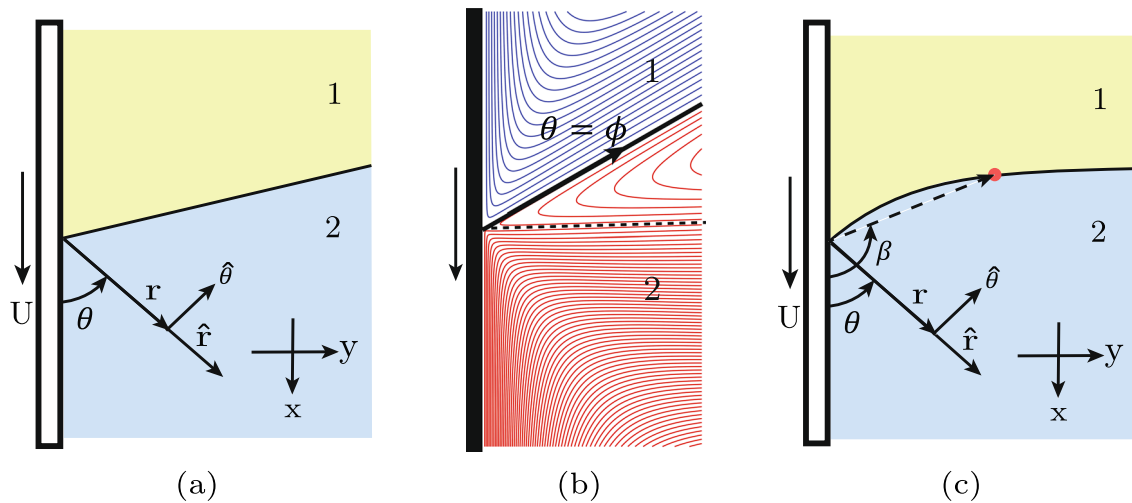


**Fig. 3** **a** Cylindrical coordinate system  $(r - \theta)$  for the flow in a wedge with origin  $(0, 0)$  at the contact line based on HS71 theory [6]. The moving plate advances from fluid-1 to fluid-2 with a speed  $U$ . **b** A typical flow pattern showing rolling motion in fluid-1 and split streamline in fluid-2 with material points along the interface  $(\theta = \phi)$  moving away from the contact line. **c** Coordinate system for local flow near a moving contact line with a curved wedge with  $\beta(r)$  varying along the curved interface

### 3 Brief review of theoretical models

The study of HS71 examined the dynamics near a moving contact line using a flat interface as shown schematically in Fig. 3a. Since curved interfaces occur in experiments, the fixed wedge angle,  $\phi$ , can simply be replaced by the variable local angle  $\beta$  [7, 11, 12]. Below, we briefly provide the analytical forms of the streamfunction as well as the interface shape based on state-of-the-art theoretical models.

#### 3.1 Models for flow fields

In the viscous limit, the two-dimensional Stokes equations reduce to the biharmonic equation for the streamfunction,  $\psi$ ,

$$\nabla^4 \psi = 0. \tag{1}$$

The analytical study of HS71 obtained a solution for the streamfunction in both fluids in terms of eight coefficients. The general solution of the streamfunction assumes the form

$$\psi_{1,2} = r(A_{1,2}(\phi) \sin \theta + B_{1,2}(\phi) \cos \theta + C_{1,2}(\phi)\theta \sin \theta + D_{1,2}(\phi)\theta \cos \theta), \tag{2}$$

where subscripts 1 and 2 denote the fluid phases. The expressions for all the coefficients are given in Appendix 1. In the HS71 formulations, the interfacial velocity,  $v_i^{HS}$ , is equal to the radial velocity at the interface and is independent of the radial location along the interface given by

$$v_i^{HS} = v_r(r, \phi) = U \left( \frac{(\phi \cos \phi - \sin \phi)(\sin^2 \phi - \delta^2) + \lambda(\delta \cos \phi - \sin \phi)(\phi^2 - \sin^2 \phi)}{\Delta} \right). \tag{3}$$

To facilitate the comparison of the streamfunction with experiments where the interface is always curved, we modify the streamfunction in Eq. (2) for a curved interface by replacing the fixed angle  $\phi$  with interface angle  $\beta(r)$  (see Fig. 3c). The local interface angle,  $\beta(r)$ , can be obtained from another model or directly measured in experiments. The streamfunction of a curved interface now becomes

$$\psi_{1,2} = r(A_{1,2}(\beta) \sin \theta + B_{1,2}(\beta) \cos \theta + C_{1,2}(\beta)\theta \sin \theta + D_{1,2}(\beta)\theta \cos \theta). \tag{4}$$

This solution is referred to as the modulated wedge solution (MWS) [11] and was shown to make excellent predictions for the flow fields when  $\lambda < 1$  [7]. The radial and tangential velocities can also be easily computed as

$$v_r(r, \theta; \beta) = \frac{\partial f}{\partial \theta}, \quad (5)$$

$$v_\theta(r, \theta; \beta) = -f - r \frac{\partial f}{\partial \beta} \frac{\partial \beta}{\partial r}, \quad (6)$$

Unlike the HS71 solution, the interfacial velocity now depends on both the radial and the angular velocities. Setting  $\theta = \beta$  in Eqs. (5) and (6), we get

$$v_i^{MWS} = v_r(r, \beta) \cos(\alpha - \beta) + v_\theta(r, \beta) \sin(\alpha - \beta). \quad (7)$$

where  $\alpha(r)$  is a measure of the slope of the interface. In the next section, we apply analytical models and show how interface shapes from theoretical models compare with experiments.

### 3.2 Models for complete interface shape

In the classical work of Cox [12], the region in the vicinity of a moving contact line was divided into three regions. The inner region, closest to the contact line was dominated by slip whereas the outer region was determined by the geometry of the problem under consideration. These two regions were matched together using the intermediate region. The well-known DRG model by Dussan et al. [13] proposed a composite solution for predicting the interface shape in the intermediate region by incorporating the static and Cox solutions to give:

$$\alpha(r) = g^{-1} \left[ g(\omega_0) + \text{Ca} \ln \left( \frac{r}{l_c} \right) \right] + (\theta_s - \omega_0), \quad (8)$$

where

$$g(x) = \int_0^x \frac{\lambda((t^2 - \sin^2 t)((\pi - t) + \sin t \cos t) + ((\pi - t)^2 - \sin^2 t)(t - \sin t \cos t))}{2 \sin t (\lambda^2(t^2 - \sin^2 t) + 2\lambda(t(\pi - t) + \sin^2 t) + ((\pi - t)^2 - \sin^2 t))} dt. \quad (9)$$

Here  $\theta_s = f_0 \left( \frac{r}{l_c}; \omega_0 \right)$  represents the static interface shape while  $\omega_0$  is interpreted as an empirical parameter in the solution that can be determined by matching the solution with the interface shape from experiments. The expression of  $f_0$  represents the two-dimensional static meniscus explained in more detail in a related study [7] and given in Appendix 2.

## 4 Results

In the present study, the flow dynamics near a moving contact line are investigated mainly at  $\lambda \geq 1$ . The following subsections discuss the results on experimental interface shapes, flow fields, and interfacial speeds along with their comparisons with available theoretical models.

### 4.1 Interface shape

Figure 4 shows a comparison of interface shape predicted by DRG solution [13] and the experiments. The matching procedure is outlined in Fig. 4a where three distinct analytical curves are shown. The static interface shape corresponds to the ‘outer’ solution characterized completely by the static contact angle. The Cox solution is the local solution valid very close to the contact line, and hence deviates from the experimental results away at distances beyond 0.3 mm from the contact line. The DRG solution, on the other hand, is a composite solution incorporating the Cox solution for small  $r$  and the static solution for large  $r$ , where  $r$  is the distance along the interface measured from the contact line. The DRG solution is parameterized in terms of a single parameter  $\omega_0$  which is determined by fitting the Eq. (8) to the experimental data. This yields  $\omega_0 \approx 64.1^\circ$ .

Figure 4b shows a comparison of three distinct liquid–liquid systems given in Table 2 against the DRG model. The DRG model is found to predict the interface shape over the whole region of the flow with just a single fitting

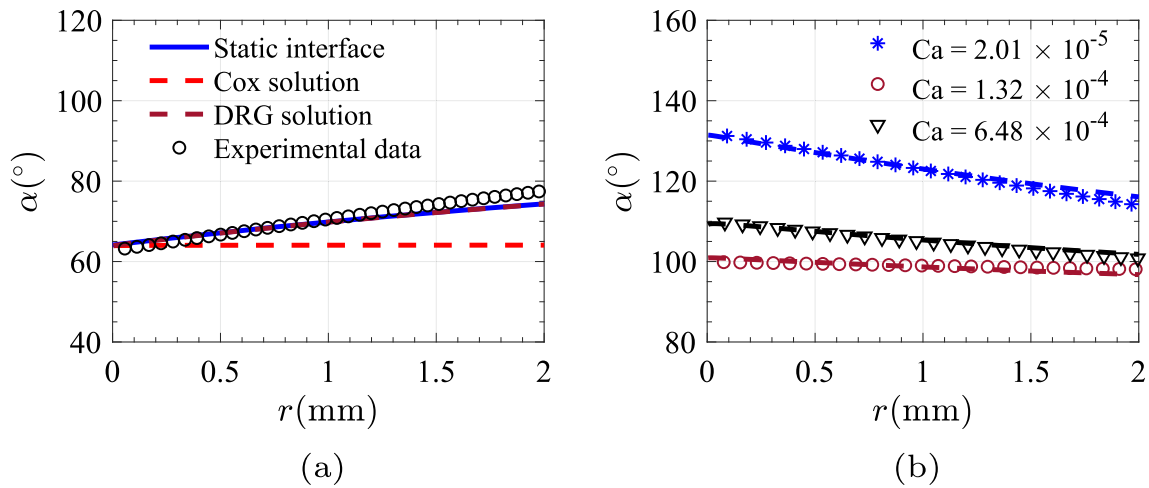


**Fig. 4** **a** A comparison of experimental interface shape with static shape (blue solid curve), Cox model (red dashed curved), and DRG model (maroon dashed curve) for combination-2 with  $Ca = 6.61 \times 10^{-5}$ . The solid surface is coated with a hydrophilic film and the DRG model results in  $\omega_0 \approx 64.1^\circ$ . **b** A comparison of interface shapes for three different model (dashed line): \*: combination-3 with  $Ca = 2.01 \times 10^{-5}$ ,  $\omega_0 \approx 131.8^\circ$ ;  $\nabla$ : combination-1 with  $Ca = 6.48 \times 10^{-4}$ ,  $\omega_0 \approx 110.4^\circ$ ;  $\circ$ : combination-2 with  $Ca = 1.32 \times 10^{-4}$ ,  $\omega_0 \approx 107.9^\circ$ . The fluid combinations are described in Table 2

parameter. The interface shape extracted from these models and experiments can be used to determine the flow field in both the fluids using the MWS theory discussed in Sect. 3 and given in Eq. (4).

### 4.2 Flow field

The key goal of this study is to determine the flow fields near a moving contact line and compare the results against theoretical predictions. The velocity field, in the form of a vector field, is obtained from PIV data. The vector field is then used to determine streamfunction using the equations

$$\frac{\partial \psi}{\partial y} = u, \quad \frac{\partial \psi}{\partial x} = -v, \tag{10}$$

by setting  $\psi = 0$  on the moving wall. Figure 5 shows a comparison between the experimentally determined streamfunction contours and theoretical predictions from MWS theory (Eq. 4). Recall that the MWS theory is a direct extension of the HS71 theory with only a small modification involving the interface angle. The solid curves represent the experimental flow field, whereas the dashed curves are obtained from theory. Given the complexity of the experiments, the agreement between theory and experiments is impressive. The HS71 theory is not only able to predict the overall shape of the flow field, but is able to make a quantitative prediction for the streamfunction field in the vicinity of the contact line. The experiments also confirm the presence of split-streamline and its location in the less viscous fluid just as predicted by HS71 theory and shown in Fig. 3b. It is important to note that no adjustable parameters were employed in the theory. To the best of our knowledge, such a detailed and direct comparison between HS71 theory and experiments in a liquid–liquid moving contact line has never been carried out before.

### 4.3 Interfacial speed

Interfacial speed ( $v_i$ ) is a tangential speed measured along the interface by projecting the experimentally determined flow field onto the interface. The direction of the interface velocity, determined from the sign of  $v_i$ , reveals the flow pattern in both the fluids. In the present study, since the glass slide is advancing downwards from silicone oil to the sugar–water mixture, a positive value of  $v_i$  corresponds to rolling motion in the upper (silicone oil) fluid and split-streamline motion in the lower (sugar–water mixture) fluid.

Figure 6 shows the interfacial speed data for 50 cSt silicone oil–sugar water mixture system. The positive value of speed indicates that fluid particles at the interface are moving away from the contact line. This is clearly consistent with the rolling motion in fluid-1 and split-streamline motion in fluid-2. The HS71 theory correctly predicts the sign of the tangential velocity, but there is clearly deviation from experimental observations.

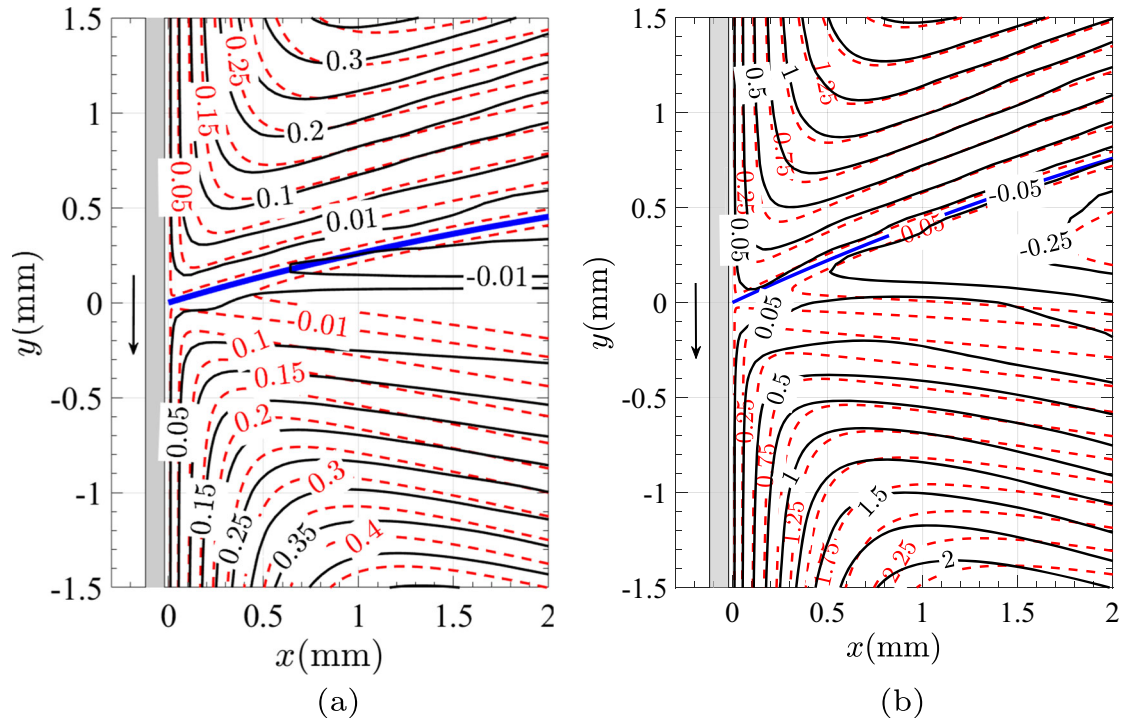


**Fig. 5** Contours of streamfunction obtained from experiments (black solid curves), MWS theory (red dashed curved) for **a** combination-2 at  $Re = 9.54 \times 10^{-1}$ , and  $Ca = 1.32 \times 10^{-4}$ , **b** combination-2 at  $Re = 4.77$ , and  $Ca = 6.61 \times 10^{-4}$ . The glass slide is coated with a hydrophilic coating. The blue solid curve represents the interface. The fluid combinations are described in Table 2

The singularity in the HS71 theory also manifests in the tangential speed given in Eq. (3), where the speed is independent of radial location from the contact line. As per HS71 theory, material points move at a constant speed along the interface since theoretical speed,  $v_i^{HS}$ , is independent of  $r$ . This indicates that material points approaching the contact line either from fluid-1 or fluid-2 instantaneously speed up (i.e. possess infinite acceleration) and then move along the interface. The experiments clearly offer a resolution to the singularity as shown in Fig. 6a. The interfacial speed is clearly shown to rapidly decrease as the contact line is approached. Hence, material points gradually accelerate and attain a constant speed as they move away from the contact line.

Another important finding of the present study is the presence of slip near the moving wall in the vicinity of the contact line as shown in Fig. 6b. Here,  $r = 0$  represents the contact line and  $r$  increases as one moves away from the contact line in fluid-2. The slip velocity is defined as the difference between the fluid and plate velocity at the moving wall normalized by the plate velocity. A value of  $v_s = 1$  represents perfect slip and  $v_s = 0$  represents no-slip. At a distance of about 1 mm away from the contact line, the no-slip boundary condition appears to be well enforced. But as one approaches the contact line, the slip velocity rapidly increases. This is another key finding of the study and offers a pathway for the resolution of the contact line singularity.

## 5 Conclusion

In this study, the velocity in the vicinity of a moving contact line in a liquid/liquid/solid system is investigated using particle image velocimetry experiments. By matching the refractive index in both liquids, the flow field in both liquids is simultaneously obtained in a single experiment. A quantitative comparison is made with theoretical models and it is shown that the theory of HS71 makes excellent predictions for flow in both liquids. To facilitate comparison between experiments and HS71 theory, the shape of the interface is determined and provided as an input to the theory which results in the modulated wedge solution (MWS). HS71 theory is also shown to make reasonable predictions for the interfacial speed. For the interface shape, the DRG model was found to make a good prediction. More sophisticated models for interface shape do exist, but these models are largely valid in the limit of  $\lambda \rightarrow 0$ , i.e. in the free-surface limit.

A key finding of the study is how the singularity in HS71 theory is arrested in the experiments. Unlike the HS71 theory, experiments clearly reveal that interface velocity rapidly varies in the vicinity of the moving contact line.



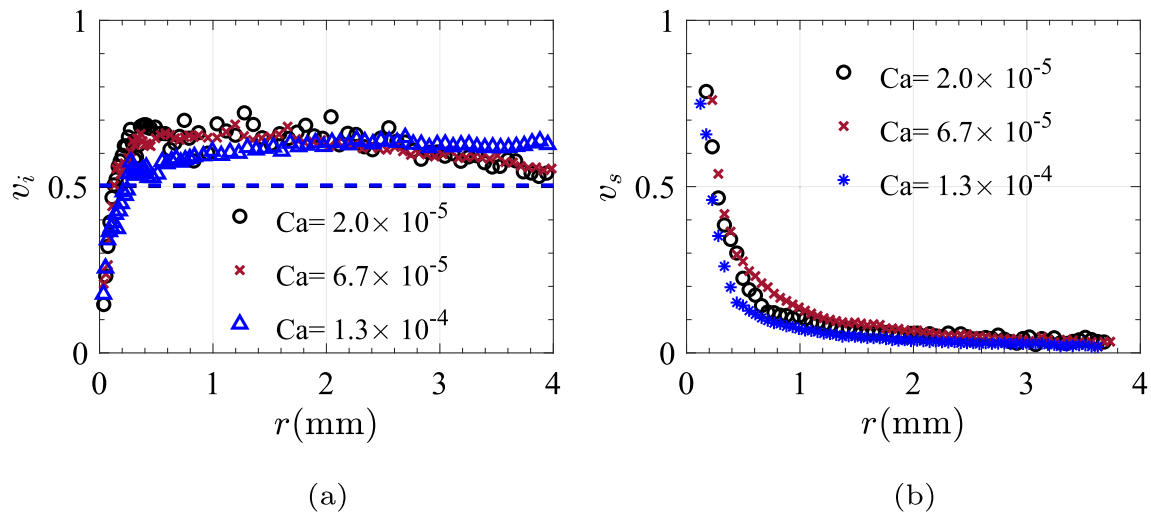


**Fig. 6** **a** A comparison of experimental interfacial speed,  $v_i$  (measured along the interface and non-dimensionalized with the speed of the plate) against HS71 theory. **b** Slip velocities (non-dimensionalized with the speed of the plate) measured in fluid-2. The data corresponds to combination-3 given in Table 2 performed over the solid surface coated with hydrophilic coating

The absence of singularity is also consistent with the presence of slip velocity along the moving wall in the vicinity of the moving contact line.

Since the viscosity ratio in the present study is close to unity, we believe the findings presented in this study will be easily amenable to numerical investigation. We hope the present study will spur new theoretical and numerical studies in liquid/liquid/solid moving contact lines.

**Acknowledgements** This work was supported by the Science and Engineering Research Board, Department of Science and Technology (DST), India (Grant number: CRG/2021/007096). The authors would also like to express their gratitude for the support received from the Fund for Improvement of Science and Technology Infrastructure (FIST) of India (Grant number: SR/FST/ETI-397/2015/(C)), and the JICA Friendship Project. The authors also thank Mr. Tejasvi Hegde and Mr. Rishab Sharma for generating some experimental data used in the paper.

**Availability of data and materials** The datasets generated during and analysed during the current study are available from the corresponding author upon reasonable request.

**Declarations**

**Conflict of interest** The authors have no conflict of interest to declare that are relevant to the content of this article.

**Appendix A: A brief description of the formulation of streamfunction in a fixed wedge**

The governing equation near a moving contact line for a fixed wedge is given as:

$$\nabla^4 \psi = 0, \tag{11}$$

where  $\psi$  can be expanded as follows:

$$\psi_{1,2} = r(A_{1,2}(\phi) \sin \theta + B_{1,2}(\phi) \cos \theta + C_{1,2}(\phi)\theta \sin \theta + D_{1,2}(\phi)\theta \cos \theta). \tag{12}$$

The eight coefficients in the above equation are determined by applying standard boundary conditions on the moving wall (no-slip) and along the interface (continuity of tangential velocity and continuity of tangential stress).

$$A_1 = \frac{1}{\sin \phi} (-C_1 \phi \sin \phi - D_1 \delta \cos \phi),$$

$$\begin{aligned}
B_1 &= -D_1\pi, \\
C_1 &= \frac{1}{\delta} \left( U - D_1 \left( \delta \frac{\cos \phi}{\sin \phi} - 1 \right) \right), \\
D_1 &= \frac{U \sin \phi \cos \phi}{\Delta} \left( (\sin^2 \phi - \delta \phi) + \lambda(\phi^2 - \sin^2 \phi) - \pi \tan \phi \right), \\
A_2 &= \frac{1}{\sin \phi} (-C_2 \phi \sin \phi - D_2 \phi \cos \phi), \\
B_2 &= 0, \\
C_2 &= \frac{1}{\phi} \left( U + D_2 \left( 1 - \phi \frac{\cos \phi}{\sin \phi} \right) \right), \\
D_2 &= \frac{U \sin \phi \cos \phi}{\Delta} \left( \sin^2 \phi - \delta^2 + \lambda(\delta \phi - \sin^2 \phi) - \lambda \pi \tan \phi \right),
\end{aligned}$$

where  $\Delta = (\sin \phi \cos \phi - \phi)(\delta^2 - \sin^2 \phi) + \lambda(\phi^2 - \sin^2 \phi)(\delta - \sin \phi \cos \phi)$  and  $\delta = \phi - \pi$ .

## Appendix B: Static interface shape in the DRG model

The static interface shape  $\theta_s$  can be described using horizontal and vertical coordinates  $H_s$  and  $X$  with the origin at the contact line as

$$\theta_s = \frac{\pi}{2} - \tan^{-1} \left( \frac{dH_s}{dX} \right). \quad (13)$$

In the above expression, the static solution is represented by subscript  $s$  and  $X \in [0, X_0]$ . A schematic for static interface shape can be seen in Fig. 7 (a dashed curve). Using the solution of the non-linear Young–Laplace equation,  $H_s(X)$ , can be written as follows:

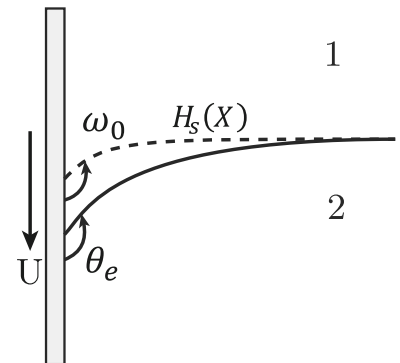
$$\begin{aligned}
H_s(X) &= \cosh^{-1} \left( \frac{2}{X_0 - X} \right) - \cosh^{-1} \left( \frac{2}{X_0} \right) \\
&\quad - (4 - (X_0 - X)^2)^{1/2} + (4 - X_0^2)^{1/2},
\end{aligned}$$

where

$$X_0 = \sqrt{2}(1 - \sin \omega_0)^{1/2}.$$

In this context,  $\omega_0$  denotes the angle at the contact line ( $x = 0$ ). Instead of being explicitly prescribed, it is determined through an iterative process that minimizes the root mean square error between the experimental interface shape and the interface shape predicted by the DRG model in Eq. (8).

**Fig. 7** A schematic shows a plate moving with speed  $U$  with respect to an interface of two immiscible fluids. The interface touches the wall at the contact line with an angle assumed to be the same as the equilibrium contact angle  $\theta_e$ .  $H_s(X)$  represents the static shape obtained by imposing a contact angle of  $\omega_0$  at the wall



## References

1. E.B. Dussan, On the spreading of liquids on solid surfaces: static and dynamic contact lines. *Ann. Rev. Fluid Mech.* **11**(1), 371–400 (1979)
2. Y. Pomeau, Recent progress in the moving contact line problem: a review. *C. R. Mec.* **330**(3), 207–222 (2002)
3. S. Yi, D. Hang, D.M.P. Spelt, Numerical simulations of flows with moving contact lines. *Ann. Rev. Fluid Mech.* **46**, 97–119 (2014)
4. H. Jacco, S.B. Andreotti, Moving contact lines: scales, regimes, and dynamical transitions. *Ann. Rev. Fluid Mech.* **45**, 269–292 (2013)
5. Y.D. Shikhmurzaev, Moving contact lines and dynamic contact angles: a ‘litmus test’ for mathematical models, accomplishments and new challenges. *Eur. Phys. J. Spec. Top.* **229**(10), 1945–1977 (2020)
6. H. Chun, L.E. Scriven, Hydrodynamic model of steady movement of a solid/liquid/fluid contact line. *J. Colloid Interface Sci.* **35**(1), 85–101 (1971)
7. G. Charul, A. Choudhury, D. Lakshmana, C.N.H. Dixit, An experimental study of flow near an advancing contact line: a rigorous test of theoretical models (2023). [arXiv:2311.09560](https://arxiv.org/abs/2311.09560)
8. M. Fermigier, P. Jenffer, An experimental investigation of the dynamic contact angle in liquid–liquid systems. *J. Colloid Interface Sci.* **146**(1), 226–241 (1991)
9. W. Zheng, B. Wen, C. Sun, B. Bai, Effects of surface wettability on contact line motion in liquid–liquid displacement. *Phys. Fluids* **33**, 0821018 (2021)
10. P. Yue, C. Zhou, J.J. Feng, Sharp-interface limit of the Cahn–Hilliard model for moving contact lines. *J. Fluid Mech.* **645**, 279–294 (2010)
11. Q. Chen, E. Ramé, S. Garoff, The velocity field near moving contact lines. *J. Fluid Mech.* **337**, 49–66 (1997)
12. R.G. Cox, The dynamics of the spreading of liquids on a solid surface. Part 1. Viscous flow. *J. Fluid Mech.* **168**, 169–194 (1986)
13. E.B. Dussan, V.E. Ramé, S. Garoff, On identifying the appropriate boundary conditions at a moving contact line: an experimental investigation. *J. Fluid Mech.* **230**, 16–97 (1991)

Springer Nature or its licensor (e.g. a society or other partner) holds exclusive rights to this article under a publishing agreement with the author(s) or other rightsholder(s); author self-archiving of the accepted manuscript version of this article is solely governed by the terms of such publishing agreement and applicable law.